Synchronization crossover of polariton condensates in weakly disordered lattices

H. Ohadi,[1,2,*] Y. del Valle-Inclan Redondo,[1] A. J. Ramsay,[3] Z. Hatzopoulos,[4] T. C. H. Liew,[5] P. R. Eastham,[6] P. G. Savvidis,[4,7,8] and J. J. Baumberg[1,†]

[1]*Department of Physics, Cavendish Laboratory, University of Cambridge, Cambridge CB3 0HE, United Kingdom*
[2]*SUPA, School of Physics and Astronomy, University of St Andrews, St Andrews, KY16 9SS, United Kingdom*
[3]*Hitachi Cambridge Laboratory, Hitachi Europe Ltd., Cambridge CB3 0HE, United kingdom*
[4]*FORTH, Institute of Electronic Structure and Laser, 71110 Heraklion, Crete, Greece*
[5]*School of Physical and Mathematical Sciences, Nanyang Technological University 637371, Singapore*
[6]*School of Physics and CRANN, Trinity College Dublin, Dublin 2, Ireland*
[7]*ITMO University, St. Petersburg 197101, Russia*
[8]*Department of Materials Science and Technology, University of Crete, 71003 Heraklion, Crete, Greece*

(Received 27 February 2018; published 8 May 2018)

We demonstrate that the synchronization of a lattice of solid-state condensates when intersite tunneling is switched on depends strongly on the weak local disorder. This finding is vital for implementation of condensate arrays as computation devices. The condensates here are nonlinear bosonic fluids of exciton-polaritons trapped in a weakly disordered Bose-Hubbard potential, where the nearest-neighboring tunneling rate (Josephson coupling) can be dynamically tuned. The system can thus be tuned from a localized to a delocalized fluid as the number density or the Josephson coupling between nearest neighbors increases. The localized fluid is observed as a lattice of unsynchronized condensates emitting at different energies set by the disorder potential. In the delocalized phase, the condensates synchronize and long-range order appears, evidenced by narrowing of momentum and energy distributions, new diffraction peaks in momentum space, and spatial coherence between condensates. Our paper identifies similarities and differences of this nonequilibrium crossover to the traditional Bose-glass to superfluid transition in atomic condensates.

DOI: 10.1103/PhysRevB.97.195109

I. INTRODUCTION

In a lattice of trapped bosons, disorder inhibits coherent tunneling, thus localizing condensation in real space. However, on-site repulsive interactions combined with a flow of bosons can tune neighboring condensates into resonance, thus enhancing tunneling through the trap barriers. This subtle interplay is crucial for understanding the rich phase diagram composed of Mott insulator, Bose glass, and superfluid, which acquires further complexity with pumping and dissipation in nonequilibrium situations. This situation is vital for understanding the capabilities of lattices of condensates to act, for instance, as quantum simulators of complex behavior. Exciton-polaritons (polaritons), which are bosons composed of an admixture of quantum-well exciton and microcavity photon [1], are an attractive system for studying the nonequilibrium Bose-Hubbard system in two dimensions [2]. A lattice potential can be achieved either structurally by depositing thin metallic films [3] and etching [4] the microcavity or by photo-injecting excitons with a spatially patterned laser [5]. In the latter case, the repulsive on-site interaction can be dynamically tuned through polariton-polariton [6] and polariton-exciton nonlinearities [7]. For single polaritons, the polariton nonlinearity is weaker than the disorder potential, but when polaritons condense into a macroscopic state, [8–10] the collective nonlinearity can be large enough to exhibit effects such as superfluidity [11,12] and solitons [13–15]. Polaritons in one condensate "puddle" can tunnel out and drive neighboring condensates [16] described through the Josephson mechanism [17]. The mechanism is more complicated with disorder-induced energy detunings between two nearest neighbors, in the case of repulsive nonlinearity [18] [Fig. 1(b)]. Here there is a critical Josephson tunneling (J_c), below which an extended condensate separates into two localized condensates at different energies, forming an unsynchronized (UNSYNC) phase. However, above J_c, the flow of polaritons from the higher-energy to the lower-energy condensate collapses their energy detuning and synchronizes (SYNC) them due to repulsive nonlinearities, as the higher-energy condensate becomes less populated and the lower-energy condensate more populated than before [see lower panel in Fig. 1(a)]. The equivalent of a Bose glass to superfluid crossover is thus expected for a nonequilibrium polariton condensate lattice in a disordered potential. This crossover occurs when the phase coherence length, which, in a disordered Bose insulator, grows with increasing density or strength of the Josephson coupling [19–21], exceeds the overall size of the lattice. The Bose glass to superfluid transition was first observed in Josephson junction arrays [22,23] and it has recently been observed in thermally equilibrated cold atom lattices [24], but different features emerge for the nonequilibrium lattice.

Here, we optically trap 25 polariton condensates inside a 5×5 square lattice within a planar semiconductor microcavity

*ho35@st-andrews.ac.uk
†jjb12@cam.ac.uk

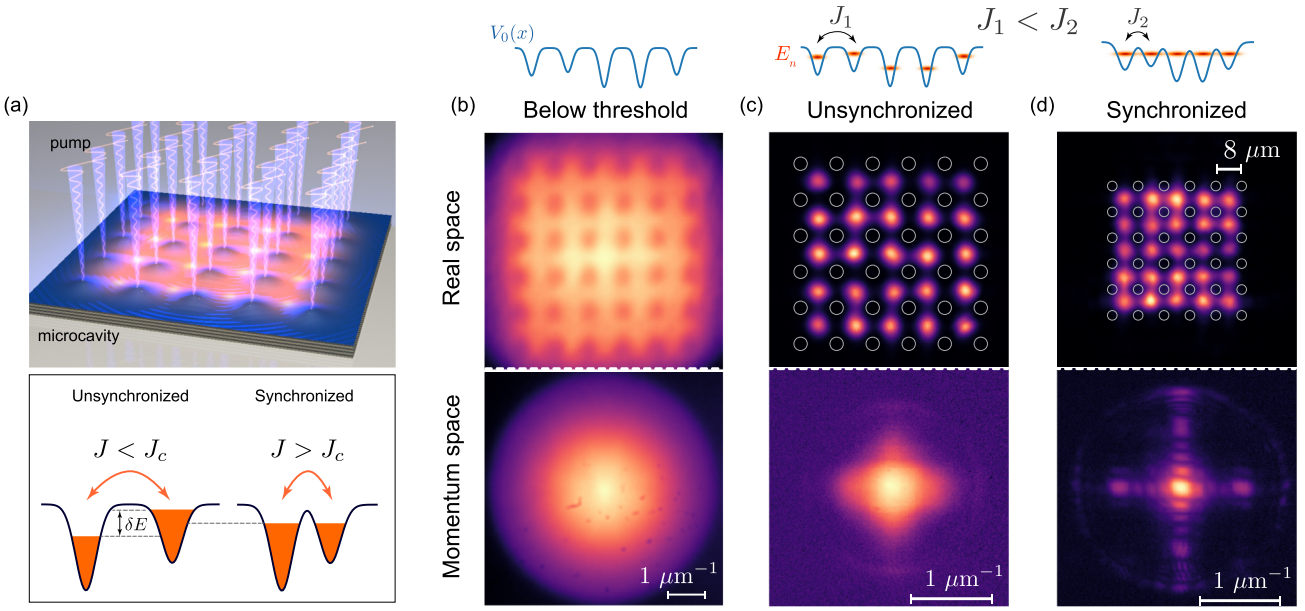

FIG. 1. Below threshold, unsynchronized, and synchronized phases. (a) Schematic of condensation in optical lattice potentials (top panel), and synchronization of two energy-detuned condensates in a double-well potential (bottom panel). There is a nonzero energy detuning δE at the UNSYNC phase but this vanishes at the SYNC phase as the Josephson coupling increases. (b)–(d) Real-space and momentum space emission of (b) uncondensed polaritons, (c) unsynchronized (localized), and (d) synchronized (delocalized) condensate lattice. Pump spots are marked by grey circles in (c), (d) and visible by dark spots in (b). The schematic diagrams above the panels show the trapping potential $V(x)$, Josephson coupling J, and energies of the condensates E_n. Momentum space images are in logarithmic scale.

[25,26] [Fig. 1(a)]. Optical trapping allows rapid and facile tuning of the lattice constant as well as the nearest-neighbor coupling strengths [27]. Due to residual weak disorder in the microcavity, polaritons at different sites condense at slightly different energies [28]. When the lattice constant is large, the nearest-neighbor coupling is small and we observe an UNSYNC phase evidenced by a broad peak in the momentum space corresponding to that of a single site condensate as well as a distribution of condensate energies, and no long-range order. However, as the nearest-neighbor coupling increases by reducing the lattice constant or increasing the condensate number density (for higher excitation powers), neighboring condensates collapse their energy detunings due to polariton-polariton and polariton-exciton nonlinearities, until they all SYNC, resulting in an extended state with long-range order. This appears as progressive narrowing of the momentum space peak and appearance of sets of diffraction peaks, signifying a phase-locked fluid with a single delocalized macroscopic wave function. Simulations show that disorder plays a key role in the crossover width and the decay of long-range order.

II. FORMATION OF TRAPPED CONDENSATES IN A DISORDERED POTENTIAL

We create polariton condensates by the nonresonant optical excitation of a microcavity composed of GaAs quantum wells sandwiched between two distributed Bragg reflectors (DBR). The cavity top (bottom) DBR is made of 32 (35) pairs of $Al_{0.15}Ga_{0.85}As$/AlAs layers of 57.2 nm/65.4 nm. Four sets of three 10 nm GaAs quantum wells separated by 10-nm-thick layers of $Al_{0.3}Ga_{0.7}As$ are placed at the maxima of the cavity light field. The $5\lambda/2$ (583 nm) cavity is made of $Al_{0.3}Ga_{0.7}As$. Photons in the cavity are strongly coupled to quantum-well excitons to form mixed light-matter bosonic polaritons.

The quasi continuous wave pump is a single-mode Ti:Sapphire laser tuned to the first Bragg mode ~100 meV above the polariton energy. A spatial light modulator is used to spatially pattern the pump beam into a square lattice. A 0.4 NA objective is used for imaging the pattern onto the sample. A cooled CCD and a 0.55 m spectrometer is used for imaging and energy resolving the emission.

The nonresonant excitation patterned in a square geometry [29] initially creates a plasma of hot electrons which then relax in energy and form bound excitons. The excitons in this "reservoir" eventually relax to form polaritons. Polaritons are repelled from reservoirs generated at each pump spot due to repulsive exciton-polariton and polariton-polariton interactions. The resulting repulsive potential causes polaritons to roll off and gather at the minima of the square potential. Polaritons condense in the ground state by stimulated scattering once the density at each center surpasses a critical threshold and form a macroscopic state in each optical trap [25,26,30].

As a single-site trapped condensate is moved across the semiconductor sample, the energy of the condensate varies by a standard deviation of ~30 μeV (see Appendix A). This ~30 μeV disorder potential is approximately 10% of the confining potential from the optical trap [26], which remains relatively constant after condensation. There is some spatial disorder in the external potential due to small inhomogeneities in the intensity pattern of the pump laser. The laser intensity disorder is ~5%, which translates to ~15 μeV of spatial disorder in the external potential, which is therefore mostly dominated by the internal disorder of the sample.

III. NARROWING OF MOMENTUM

Condensate lattices are created by patterning the optical excitation into a square lattice of 6×6 Gaussian spots [marked by grey circles in Figs. 1(c) and 1(d)] using a spatial light modulator. The lattice constant (a) of the trapping potential can be continuously varied while monitoring the total emission of the condensate lattice in momentum space (see also Supplemental Material [31]). At low excitation powers, incoherent polaritons confined by the highest points of the lattice potential [dark spots in Fig. 1(b)] are created with a very broad momentum distribution (full width half max $= \delta k \simeq 2.1\,\mu\mathrm{m}^{-1}$, k is the in-plane polariton momentum). At a threshold power ($P = P_{\mathrm{th}}$), polaritons condense in the lattice sites. When the condensates are far apart ($a > 12\,\mu$m) and the coupling between them is small, we observe a broad peak ($\delta k \simeq 0.5\,\mu\mathrm{m}^{-1}$) centered at zero momentum with no structure, and of a similar width to the emission from a single condensate [Fig 1(c)]. However, this changes as the lattice constant is reduced to $a \simeq 8\,\mu$m when a new diffraction pattern is observed. It has a narrow center peak ($\delta k \simeq 0.14\,\mu\mathrm{m}^{-1}$), with four primary interference maxima at opposite corners of the reciprocal lattice with $\mathbf{k} \cdot \mathbf{a} = 2\pi \times 0.96$, suggesting the lattice is phase locked [Fig. 1(d), and also Appendix B].

Tracking the width of the zero-momentum peak (δk) with lattice constant (a) reveals the synchronization crossover (Fig. 2). For $a > 12\,\mu$m, the condensates are weakly coupled and δk is fixed to that of a single lattice site. For $8 < a < 12\,\mu$m, δk reduces as the lattice constant a decreases until reaching a value of $\delta k \cdot a \sim 1$ at $a = 8\,\mu$m. This is the value expected for a five-slit diffraction grating, indicating phase coherence across the entire 5×5 lattice (see Appendix B). For smaller separations, $\delta k \cdot a$ remains constant until $a \simeq 4\,\mu$m, where the trap size becomes comparable to the reservoir width. In this regime, the traps merge into a single large inhomogeneous pump spot.

The power dependence of δk for a fixed lattice constant ($a = 8\,\mu$m) shows the evolution of the long-range coherence with increasing density—Fig. 2(b), also Supplemental Material [32]. We compare this to emission from a single condensate using spatial filtering for the same conditions. As the lattice power approaches the single-site condensation threshold ($P = P_{\mathrm{th}}$), polaritons condense in each lattice site and δk drops sharply. At threshold, there is a condensate at each site and the zero-momentum peak has a width similar to that of the spatially filtered single condensate, δk_1. This is because there is no long-range phase correlation and the lattice is in the UNSYNC phase. However, as power increases further, δk gradually decreases until it plateaus to $\delta k \simeq \delta k_1/4$, at $P \simeq 2P_{\mathrm{th}}$. This value again matches with a five-slit grating, indicating long-range phase correlation of a delocalized fluid across the entire lattice.

IV. BUILDUP OF LONG-RANGE COHERENCE AND COLLAPSE OF ENERGY DETUNING

The gradual decrease in momentum width δk with power implies that phase correlations in the lattice continuously increase with power as the coherence length of the order parameter ψ gradually increases. It has been shown that

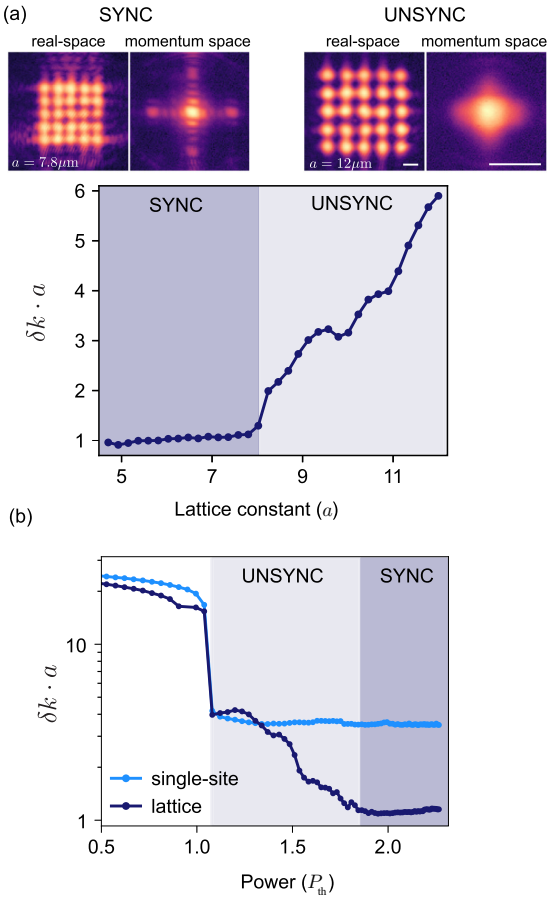

FIG. 2. Synchronization phase diagram. Dependence of $\delta k \cdot a$ versus (a) lattice constant and (b) power. Top panel in (a) shows real-space and momentum-space intensity (log scale) at $a = 7.8\,\mu$m (left) and $a = 11.8\,\mu$m for $P = 2.1P_{\mathrm{th}}$. (b) Power dependence comparison of $\delta k \cdot a$ for full lattice (dark blue) and a spatially filtered single condensate (light blue). Real-space scale is $10\,\mu$m and momentum space scale is $1\,\mu\mathrm{m}^{-1}$.

in a driven-dissipative condensate with disorder, the phase correlation length $\mathcal{L}_\phi$, over which the first-order correlation function drops by $1/e$, increases with Josephson coupling and condensate density [20]. To confirm this, we measure the spatial first-order coherence function $g^{(1)}$ at zero time delay. The lattice emission is sent to a modified Mach-Zehnder interferometer with a retroreflector in one arm. This interferes emission from opposite points relative to the central condensate [placing the origin at the white dashed circle in Fig. 3(a)] so that emission from r interferes with $-r$. The contrast of these interferograms then gives $|g^{(1)}(r,-r)| = |g^{(1)}(-r,r)|$, with $\mathcal{L}_\phi$ being the phase correlation length where $g^{(1)}$ drops to $1/e$. The interferograms [Fig. 3(a)] clearly differ between the localized (top panel, $P = 1.4P_{\mathrm{th}}$) and the delocalized phase (bottom panel, $P = 2P_{\mathrm{th}}$). Single-site coherence builds up immediately after condensation. However, the coherence between different lattice sites turns on at a power that increases with separation (see also Supplemental Material [33]). This first-order spatial coherence function $g^{(1)}(-r,r)$ clearly changes at different powers [Fig. 3(b)]. Before condensation ($P < P_{\mathrm{th}}$), $\mathcal{L}_\phi \simeq 0$. At single-site condensation (UNSYNC, $P = 1.1P_{\mathrm{th}}$), order

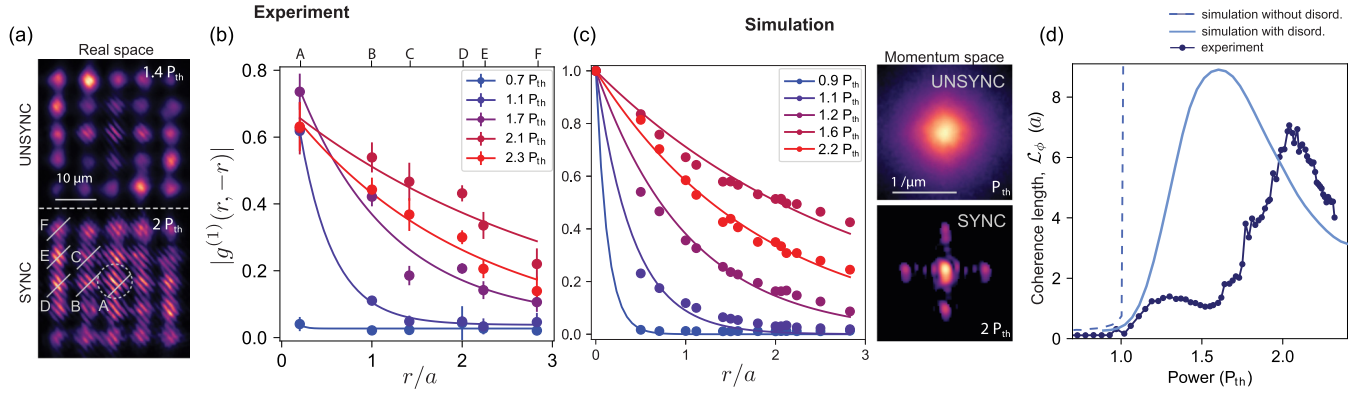

FIG. 3. First-order correlation function. (a) Real-space interferograms for the unsynchronized (top) and synchronized (bottom) phases. (b), (c) Power dependence of $|g^{(1)}(r,-r)|$ at various lattice positions r, as a function of total lattice power in (b) experiment and (c) simulations. Lines are exponential fits. In the experiment, an average is taken over six site separations marked A–F and their corresponding mirrors in (a), with separations of $(0.5,2,\sqrt{2},4,2\sqrt{5},4\sqrt{2})a$. In simulations, the average is extracted for all site separations in the lattice. Lines are exponential fits. Panels to the right of (c) are the time-averaged momentum space emission for UNSYNC ($P = P_{\rm th}$) and SYNC ($P = 2P_{\rm th}$) phases. The simulated disorder ratio is 10%. (d) Coherence length ($\mathcal{L}_\phi$) versus power in simulations (with and without 10% disorder) and in experiment. Simulation curves are averages of 25 randomly generated disorder potentials.

is confined to one site. As power increases ($1.1P_{\rm th} < P < 2.1P_{\rm th}$), $\mathcal{L}_\phi$ increases gradually until it reaches ~8 lattice constants (at $P = 2.1P_{\rm th}$), but decays at higher powers due to the appearance of higher-order modes [Fig. 3(d)]. We note that the increase of $g^{(1)}$ (and the reduction of δk) in steps is likely due to a percolation effect where domains of condensates phase-lock in discrete steps.

Measuring the site energies of condensates in the synchronization crossover reveals the reason behind this behavior. At threshold, condensates form at slightly different energies [Fig. 4(a)]. The energy distribution observed in the UNSYNC phase is a result of spatial inhomogeneities in the sample. However, as the power increases, the condensate energies converge as long-range order propagates across the lattice, and at the SYNC phase they condense to one energy [Fig. 4(b)].

V. THEORETICAL MODEL AND NUMERICAL SIMULATIONS

Our system can be modeled using the stochastic driven-dissipative Gross-Pitaevskii (GP) equation, which is a nonlinear Schrödinger equation including pumping, dissipation, energy relaxation, and Langevin noise to describe fluctuations:

$$i\hbar\frac{d\psi}{dt} = \left(-\frac{\hbar^2\nabla^2}{2m} + V_0 + g_R n + g_p P + \alpha|\psi|^2\right)\psi, + \frac{i}{2}(\hbar R n - \hbar\gamma)\psi - i\hbar\Lambda\psi + \hbar\sqrt{\gamma + Rn}\frac{dW}{dt}, \tag{1}$$

$$\frac{dn}{dt} = P - (\gamma_R + R|\psi|^2)n. \tag{2}$$

Here, ψ is the wave function, n is the reservoir density, m is the polariton mass, R is the scattering rate from the reservoir to the condensate, γ is the polariton decay rate, g_R and g_p describe energy repulsion due to the presence of the reservoir and pump, α is the strength of polariton-polariton interactions, P is the nonresonant pumping rate, γ_R is the reservoir decay rate, and Λ is a spatial-dependent function matching the pump profile, which accounts for a phenomenological energy relaxation. The spatio-temporal Langevin noise is given by dW, which is a two-dimensional complex Gaussian random variable characterized by correlation function $\langle dW_x^* dW_{x'}\rangle = dt\delta_{x,x'}$, where x and x' are the vector coordinates of the grid points. Here, we also add a static disorder potential V_0, accounting for the sample inhomogeneity. Disorder ratio (DOR) is defined as DOR $= \overline{V_0}/(g_R n + g_P P + \alpha|\psi|^2)$. The first-order correlation function is given by

$$g^{(1)}(\mathbf{r},-\mathbf{r}) = \frac{\langle\psi(\mathbf{r})^*\psi(-\mathbf{r})\rangle}{\sqrt{\langle|\psi(\mathbf{r})|^2\rangle\langle|\psi(-\mathbf{r})|^2\rangle}}. \tag{3}$$

Simulating the condensate lattice in a randomly generated disorder potential demonstrates the crucial role of disorder in the synchronization crossover, as shown in Fig. 5 [34]. Here, the DOR, defined as the mean ratio of a Gaussian-distributed disorder potential [Fig. 5(g)] to the confinement potential by the pump pattern, is ~10% (as in the experiment), and we plot the steady state time-averaged densities. The condensate lattice crosses from UNSYNC to SYNC as the lattice

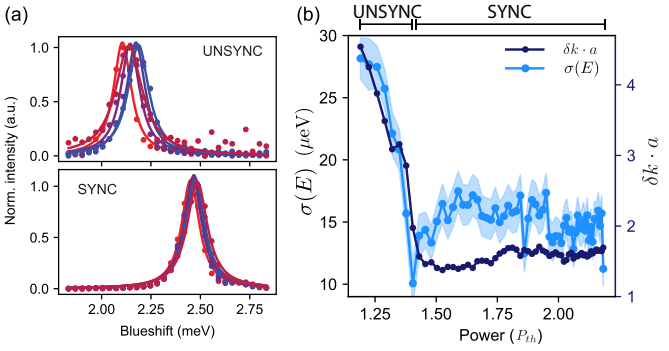

FIG. 4. Condensate energies as a function of power. (a) Energy spectra of a column of five condensates crossing the center of the lattice for $P = P_{\rm th}$ (top panel) and $P = 2P_{\rm th}$ (bottom panel). (b) Standard deviation of condensate energies ($\sigma(E)$) as a function of power (light blue) and the corresponding $\delta k \cdot a$ (dark blue).

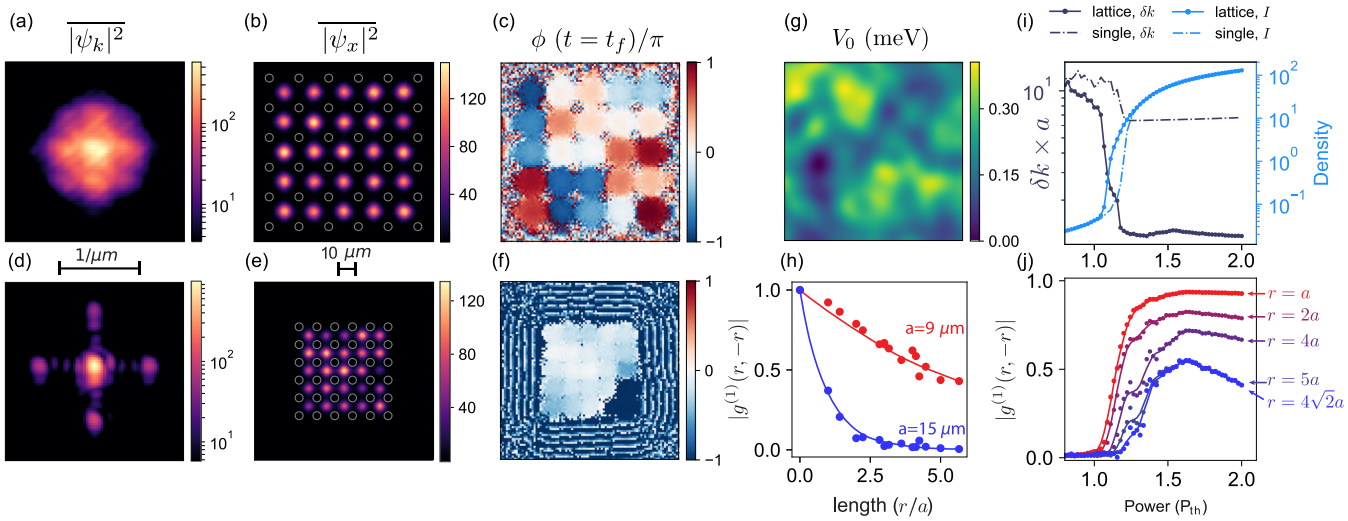

FIG. 5. Time-averaged momentum space, real space, and phase of an unsynchronized lattice (a)–(c) and synchronized lattice (d)–(f). (g) Static potential accounting for sample inhomogeneity. (h) $g^{(1)}$ versus length for UNSYNC (blue) and SYNC phase (red). (i) Power dependence of density (light blue) and momentum width (dark blue) for a synchronized lattice (solid line) and a single site (dotted line) for $a = 9\,\mu$m. (j) Power dependence of $g^{(1)}$ for different lattice lengths for $a = 9\,\mu$m.

constant is shrunk, with similar signatures to the experiment. In the UNSYNC phase, when $a = 15\,\mu$m [Figs. 5(a)–5(c)], the momentum-space peak is broad, condensate phases are unlocked and $\mathcal{L}_\phi \simeq a$ [blue line in Fig. 5(h)]. This changes in the SYNC phase as the lattice is shrunk to $a = 9\,\mu$m: the momentum-space peak narrows and new diffraction peaks appear, condensates phase-lock [Figs. 5(d)–5(f)], and $\mathcal{L}_\phi$ goes beyond the lattice dimensions (red line in Fig. 5(h)]. The power dependence of the SYNC lattice shows gradual narrowing of the momentum peak and buildup of long-range coherence [Figs. 5(i) and 5(j)].

We find that the power dependence of the correlation function strongly depends on the spatial profile of the disorder potential. For this reason, $|g^{(1)}|$ simulations are averaged for 25 randomly generated disorder potentials, as shown in Fig. 3(c). The general trend stays the same: in the UNSYNC phase, $g^{(1)}$ does not expand beyond a single site, whereas in the SYNC phase, $g^{(1)}$ builds up throughout the lattice with an exponential drop off [Figs. 3(c) and 3(d)] (see Appendix C for larger lattices). In the SYNC phase, the Josephson coupling is strong enough to overcome the disorder potential and phase lock the condensates to form a single macroscopic state. Without static disorder, this synchronization crossover is sharp and the coherence length is 3 orders of magnitude longer than in the experiment [Fig. 3(d)]. The minimization of the width of this synchronization crossover with power can thus be used to search for an optical potential that minimizes the static disorder potential, which has applications in enabling using such arrays as simulators. We note that disorder is inherent to any supported array of condensates, suggesting these observations will be universal to all implementations.

VI. CONCLUDING REMARKS

We demonstrated a controllable crossover from UNSYNC to SYNC in a driven-dissipative polariton condensate lattice with a background disorder potential. The crossover occurs either by increasing the density of all condensates or the nearest-neighbor Josephson coupling. The SYNC (delocalized) phase is accompanied by the appearance of long-range order and narrowing of the central peak in momentum space, whereas in the UNSYNC phase, order remains local, and the momentum space resembles the emission from a single condensate. Using simulations of driven-dissipative GP equations, we find that in the absence of disorder, a sharp synchronization transition with long-range spatial coherence is observed. However, the introduction of disorder results in a softer crossover from UNSYNC to SYNC regimes with finite range for the spatial coherence.

In thermalized cold atoms in a spatially disordered Bose-Hubbard potential, there is the compressible Bose-glass (insulator) crossover phase between the Mott insulator and superfluid phases [23,24,35,36]. There, although the condensates share a global chemical potential, there is no long-range spatial coherence. Instead, the system forms puddles or domains of coherent condensates, but there is no coherence between neighboring puddles. As the tunneling rate exceeds the disorder potential, the superfluid puddles coalesce until there exists a global superfluid with a spatial coherence length that exceeds the size of the system.

By contrast, in the nonequilibrium case studied here, in the crossover regime the puddles or domains have different chemical potentials or emission energies. Furthermore, in the superfluid phase, the spatial coherence has a finite range that increases with pump power and tunneling rate. Hence driven-dissipative generalization of superfluidity can only be observed in a system of finite size, as discussed theoretically in Ref. [20]. Unless actively compensated [28], this may have consequences for the scale-up of simulators based on lattices of exciton-polariton condensates.

With our capability to optically compensate for disorder [28], it would be interesting to study the interplay between on-demand disorder strengths and the synchronization crossover, and their relation to the characteristic length-scales of the

first-order spatial correlation. In addition to fundamental interest, synchronization of arrays of polariton lasers for example, would be advantageous for creating high-power density coherent sources at low pump density. Conventional laser diodes locked by injection coupling can SYNC only in a narrow range of parameters [37], due to their large carrier-induced redshift. By contrast, we demonstrate that with a carrier-induced blueshift, synchronization readily occurs, suggesting that polariton laser approaches may be highly profitable.

ACKNOWLEDGMENTS

We thank Jonathan Keeling, Peter Kirton and Ulrich Schneider for fruitful discussions. We acknowledge Grants No. EPSRC EP/L027151/1, ERC LINASS No. 320503, and Leverhulme Trust Grant No. VP1-2013-011. P.S. acknowledges support from ITMO Fellowship Program and Megagrant No. 14.Y26.31.0015 of the Ministry of Education and Science of Russian Federation and Polisimulator project cofinanced by Greece and the EU Regional Development Fund. P.E. acknowledges support from SFI Grant No. 15/IACA/3402. T.L. was supported by the Ministry of Education (Singapore) (MOE2017-T2-1-001).

The raw data supporting this paper is available in [38].

APPENDIX A: DISORDER POTENTIAL

The background disorder potential V_0 is measured experimentally by moving a single trapped condensate over the sample and measuring its energy, as shown in Fig. 6. The standard deviation of the disorder potential is $\sim 29\,\mu$eV.

APPENDIX B: PHENOMENOLOGICAL MODEL

Let us assume a coherent superposition of Gaussian wave functions localized at each lattice point:

$$A\sum_{n,m} e^{-((x-na)^2+(y-ma)^2)/(2L^2)}, \tag{B1}$$

where A is an overall amplitude, a is the lattice constant, and L defines the width of each Gaussian. In reciprocal space, the wave function is given by the Fourier transform:

$$\begin{aligned}\tilde{\psi}(k_x,k_y) &= \frac{1}{2\pi}\int_{-\infty}^{\infty}\int_{-\infty}^{\infty}\psi(x,y)e^{i(k_x x+k_y y)}dxdy \\ &= AL^2 e^{-(k_x^2+k_y^2)L^2/2}\sum_{n,m} e^{ia(k_x n+k_y m)}.\end{aligned} \tag{B2}$$

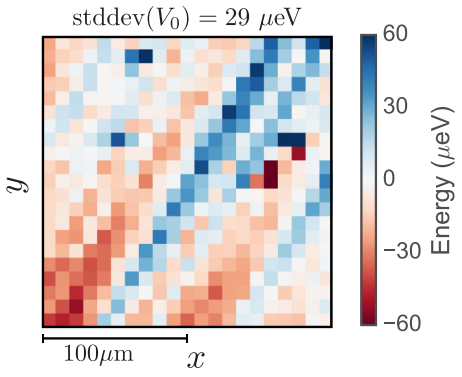

FIG. 6. Background disorder potential.

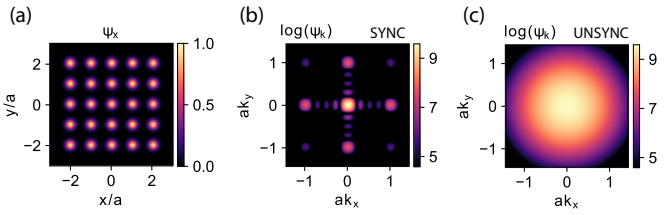

FIG. 7. (a) Intensity in real space. (b) Intensity of the SYNC phase in momentum space. (c) Intensity of the UNSYNC phase in momentum space. The only parameter is $L/a = 0.22$.

The corresponding intensities of the wave functions in real and reciprocal space are shown in Fig. 7. In the UNSYNC phase, there is no coherence between different Gaussian spots. In this case, the intensity in real space is given by

$$I(x,y) = |A|^2\sum_{n,m} e^{-((x-na)^2+(y-ma)^2)/L^2}. \tag{B3}$$

The intensity in reciprocal space is obtained taking the Fourier transform of each Gaussian spot separately, and summing the intensities rather than the amplitudes:

$$\tilde{I}(k_x,k_y) = NM|A|^2L^4 e^{-(k_x^2+k_y^2)/L^2}. \tag{B4}$$

Since there is no coherence between Gaussian spots, the interference term appearing in Eq. (B2) is no longer present in Eq. (B4). The sum over n and m has been reduced to the total number of spots, NM, in the square lattice. The corresponding intensity of the wave functions in the momentum space is shown in Fig. 7(c). This model obviously cannot describe why the crossover is not sharp and why the coherence length decays over length. For that, we model the system using a stochastic driven-dissipative GP equation.

We note here the similarities between the SYNC lattice intensity profile, and Fraunhofer diffraction from many slits given by [39]

$$I = I_0\left(\frac{\sin\beta}{\beta}\right)^2\left(\frac{\sin N\alpha}{\sin\alpha}\right)^2, \tag{B5}$$

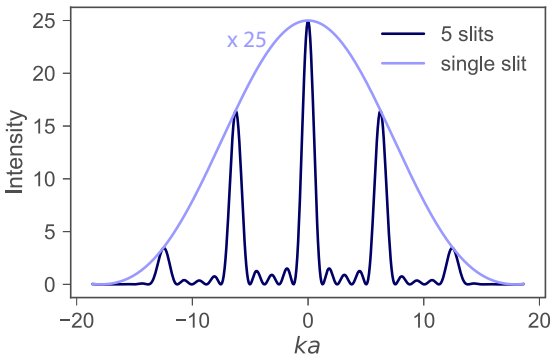

FIG. 8. Fraunhofer diffraction of a single slit (light blue) and five slits (dark blue) with $b/a = 0.35$.

where $\beta = \frac{1}{2}k_{\parallel}b$, $\alpha = \frac{1}{2}k_{\parallel}a$. Here, a is the slit separation, b is the slit width, N is the number of slits, and I_0 includes all the constants to give maximum intensity from a single slit (Fig. 8). From Eq. (B5), we can see that the first intensity minimum occurs at $ka = 2\pi/N$. For five slits, the full width at half maximum of the center peak is $\delta k \cdot a \simeq 1.13$.

APPENDIX C: LARGE LATTICE SIMULATIONS WITH DISORDER

The dependence of the first-order correlation function with the lattice constant for a 15×15 lattice in a random disorder potential (DOR = 10%) shows an exponential decay with a coherence length $\mathcal{L}_\phi$, which grows as the lattice constant a reduces, as shown in Fig. 9.

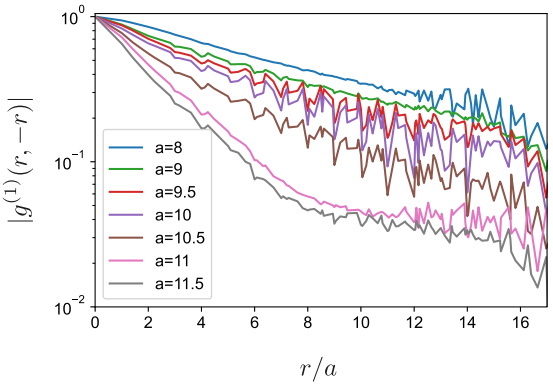

FIG. 9. Average first-order correlation function $g^{(1)}(r/a)$ versus length r for various lattice constants of a 15×15 condensate lattice.

[1] A. V. Kavokin, J. Baumberg, G. Malpuech, and F. P. Laussy, *Microcavities* (Oxford University Press, Oxford, 2007).

[2] I. Carusotto and C. Ciuti, Quantum fluids of light, Rev. Mod. Phys. **85**, 299 (2013).

[3] C. W. Lai, N. Y. Kim, S. Utsunomiya, G. Roumpos, H. Deng, M. D. Fraser, T. Byrnes, P. Recher, N. Kumada, T. Fujisawa, and Y. Yamamoto, Coherent zero-state and [pgr]-state in an exciton-polariton condensate array, Nature **450**, 529 (2007).

[4] M. Galbiati, L. Ferrier, D. D. Solnyshkov, D. Tanese, E. Wertz, A. Amo, M. Abbarchi, P. Senellart, I. Sagnes, A. Lemaître, E. Galopin, G. Malpuech, and J. Bloch, Polariton Condensation in Photonic Molecules, Phys. Rev. Lett. **108**, 126403 (2012).

[5] E. Wertz, L. Ferrier, D. D. Solnyshkov, R. Johne, D. Sanvitto, A. Lemaître, I. Sagnes, R. Grousson, A. V. Kavokin, P. Senellart, G. Malpuech, and J. Bloch, Spontaneous formation and optical manipulation of extended polariton condensates, Nat. Phys. **6**, 860 (2010).

[6] N. Takemura, S. Trebaol, M. Wouters, M. T. Portella-Oberli, and B. Deveaud, Polaritonic feshbach resonance, Nat. Phys. **10**, 500 (2014).

[7] T. Gao, P. S. Eldridge, T. C. H. Liew, S. I. Tsintzos, G. Stavrinidis, G. Deligeorgis, Z. Hatzopoulos, and P. G. Savvidis, Polariton condensate transistor switch, Phys. Rev. B **85**, 235102 (2012).

[8] H. Deng, G. Weihs, C. Santori, J. Bloch, and Y. Yamamoto, Condensation of semiconductor microcavity exciton polaritons, Science **298**, 199 (2002).

[9] J. Kasprzak, M. Richard, S. Kundermann, A. Baas, P. Jeambrun, J. M. J. Keeling, F. M. Marchetti, M. H. Szymańska, R. André, J. L. Staehli *et al.*, Bose-Einstein condensation of exciton polaritons, Nature **443**, 409 (2006).

[10] J. Baumberg, A. Kavokin, S. Christopoulos, A. Grundy, R. Butté, G. Christmann, D. Solnyshkov, G. Malpuech, G. B. H. von Högersthal, E. Feltin *et al.*, Spontaneous Polarization Buildup in a Room-Temperature Polariton Laser, Phys. Rev. Lett. **101**, 136409 (2008).

[11] A. Amo, J. Lefrère, S. Pigeon, C. Adrados, C. Ciuti, I. Carusotto, R. Houdré, E. Giacobino, and A. Bramati, Superfluidity of polaritons in semiconductor microcavities, Nat. Phys. **5**, 805 (2009).

[12] G. Lerario, A. Fieramosca, F. Barachati, D. Ballarini, K. S. Daskalakis, L. Dominici, M. De Giorgi, S. A. Maier, G. Gigli, S. Kéna-Cohen, and D. Sanvitto, Room-temperature superfluidity in a polariton condensate, Nat. Phys. **13**, 837 (2017).

[13] A. Amo, S. Pigeon, D. Sanvitto, V. G Sala, R. Hivet, I. Carusotto, F. Pisanello, G. Leménager, R. Houdré, E. Giacobino, C. Ciuti, and A. Bramati, Polariton superfluids reveal quantum hydrodynamic solitons, Science **332**, 1167 (2011).

[14] M. Sich, D. N. Krizhanovskii, M. S. Skolnick, A. V. Gorbach, R. Hartley, D. V. Skryabin, E. A. Cerda-Méndez, K. Biermann, R. Hey, and P. V. Santos, Observation of bright polariton solitons in a semiconductor microcavity, Nature Photonics **6**, 50 (2012).

[15] P. M. Walker, L. Tinkler, B. Royall, D. V. Skryabin, I. Farrer, D. A. Ritchie, M. S. Skolnick, and D. N. Krizhanovskii, Dark Solitons in High Velocity Waveguide Polariton Fluids, Phys. Rev. Lett. **119**, 097403 (2017).

[16] A. Baas, K. G. Lagoudakis, M. Richard, R. André, L. S. Dang, and B. Deveaud-Plédran, Synchronized and Desynchronized Phases of Exciton-Polariton Condensates in the Presence of Disorder, Phys. Rev. Lett. **100**, 170401 (2008).

[17] K. G. Lagoudakis, B. Pietka, M. Wouters, R. André, and B. Deveaud-Plédran, Coherent Oscillations in an Exciton-Polariton Josephson Junction, Phys. Rev. Lett. **105**, 120403 (2010).

[18] M. Wouters, Synchronized and desynchronized phases of coupled nonequilibrium exciton-polariton condensates, Phys. Rev. B **77**, 121302 (2008).

[19] G. Malpuech, D. D. Solnyshkov, H. Ouerdane, M. M. Glazov, and I. Shelykh, Bose Glass and Superfluid Phases of Cavity Polaritons, Phys. Rev. Lett. **98**, 206402 (2007).

[20] A. Janot, T. Hyart, P. R. Eastham, and B. Rosenow, Superfluid Stiffness of a Driven Dissipative Condensate with Disorder, Phys. Rev. Lett. **111**, 230403 (2013).

[21] B. Nelsen, G. Liu, M. Steger, D. W. Snoke, R. Balili, K. West, and L. Pfeiffer, Dissipationless Flow and Sharp Threshold of a Polariton Condensate with Long Lifetime, Phys. Rev. X **3**, 041015 (2013).

[22] L. J. Geerligs, M. Peters, L. E. M. de Groot, A. Verbruggen, and J. E. Mooij, Charging Effects and Quantum Coherence in Regular Josephson Junction Arrays, Phys. Rev. Lett. **63**, 326 (1989).

[23] M. P. A. Fisher, P. B. Weichman, G. Grinstein, and D. S. Fisher, Boson localization and the superfluid-insulator transition, Phys. Rev. B **40**, 546 (1989).

[24] C. Meldgin, U. Ray, P. Russ, D. Chen, D. M. Ceperley, and B. DeMarco, Probing the Bose glass-superfluid transition using quantum quenches of disorder, Nat. Phys. **12**, 646 (2016).

[25] P. Cristofolini, A. Dreismann, G. Christmann, G. Franchetti, N. G. Berloff, P. Tsotsis, Z. Hatzopoulos, P. G. Savvidis, and J. J. Baumberg, Optical Superfluid Phase Transitions and Trapping of Polariton Condensates, Phys. Rev. Lett. **110**, 186403 (2013).

[26] A. Askitopoulos, H. Ohadi, A. V. Kavokin, Z. Hatzopoulos, P. G. Savvidis, and P. G. Lagoudakis, Polariton condensation in an optically induced two-dimensional potential, Phys. Rev. B **88**, 041308 (2013).

[27] H. Ohadi, Y. del V.-I. Redondo, A. Dreismann, Y. G. Rubo, F. Pinsker, S. I. Tsintzos, Z. Hatzopoulos, P. G. Savvidis, and J. J. Baumberg, Tunable Magnetic Alignment Between Trapped Exciton-Polariton Condensates, Phys. Rev. Lett. **116**, 106403 (2016).

[28] H. Ohadi, A. J. Ramsay, H. Sigurdsson, Y. del V.-I. Redondo, S. I. Tsintzos, Z. Hatzopoulos, T. C. H. Liew, I. A. Shelykh, Y. G. Rubo, P. G. Savvidis, and J. J. Baumberg, Spin Order and Phase Transitions in Chains of Polariton Condensates, Phys. Rev. Lett. **119**, 067401 (2017).

[29] H. Ohadi, A. Dreismann, Y. G. Rubo, F. Pinsker, Y. del V.-I. Redondo, S. I. Tsintzos, Z. Hatzopoulos, P. G. Savvidis, and J. J. Baumberg, Spontaneous spin bifurcations and ferromagnetic phase transitions in a spinor exciton-polariton condensate, Phys. Rev. X **5**, 031002 (2015).

[30] P. Tsotsis, P. S. Eldridge, T. Gao, S. I. Tsintzos, Z. Hatzopoulos, and P. G. Savvidis, Lasing threshold doubling at the crossover from strong to weak coupling regime in GaAs microcavity, N. J. Phys. **14**, 023060 (2012).

[31] See Supplemental Material at http://link.aps.org/supplemental/10.1103/PhysRevB.97.195109 for URL 1, video of lattice constant dependence.

[32] See Supplemental Material at http://link.aps.org/supplemental/10.1103/PhysRevB.97.195109 for URL 2, vVideo of power scan.

[33] See Supplemental Material at http://link.aps.org/supplemental/10.1103/PhysRevB.97.195109 for URL 3, video of long-range coherence power dependence.

[34] Parameters, $\alpha = 3\,\mu\text{eV}\,\mu\text{m}^2$, $g_r = 2\alpha$, $g_P = 0.6\alpha$, $\Lambda = 0.2\ \text{ps}^{-1}$, $m^* = 5.1 \times 10^{-5}\,m_e$ where m_e is the free electron mass, $R = 0.01\,\text{ps}^{-1}\,\mu\text{m}^2$, $\gamma = 0.1\,\text{ps}^{-1}$, $\gamma_R = 62.5\gamma$.

[35] W. Krauth, N. Trivedi, and D. Ceperley, Superfluid-Insulator Transition in Disordered Boson Systems, Phys. Rev. Lett. **67**, 2307 (1991).

[36] L. Fallani, J. E. Lye, V. Guarrera, C. Fort, and M. Inguscio, Ultracold Atoms in a Disordered Crystal of Light: Towards a Bose Glass, Phys. Rev. Lett. **98**, 130404 (2007).

[37] H. G. Winful and S. S. Wang, Stability of phase locking in coupled semiconductor laser arrays, Appl. Phys. Lett. **53**, 1894 (1988).

[38] https://doi.org/10.17863/CAM.22783.

[39] M. Born, E. Wolf, A. B. Bhatia, P. C. Clemmow, D. Gabor, A. R. Stokes, A. M. Taylor, P. A. Wayman, and W. L. Wilcock, *Principles of Optics: Electromagnetic Theory of Propagation, Interference and Diffraction of Light* (Cambridge University Press, Cambridge, 1999).